https://doi.org/10.5194/gmd-2023-236
Preprint. Discussion started: 8 January 2024

Geoscientific Model Development Discussions

Development of a total variation diminishing (TVD) Sea ice transport scheme and its application in in an ocean (SCHISM v5.11) and sea ice (Icepack v1.3.4) coupled model on unstructured grids

Qian Wang[1,2], Fei Chai[1,2,3], Yang Zhang[2], Y. Joseph Zhang[4], Lorenzo Zamperi[5]

1. School of Oceanography, Shanghai Jiao Tong University, Shanghai, China
2. State Key Laboratory of Satellite Ocean Environment Dynamics, Second Institute of Oceanography, Ministry of Natural Resources, Hangzhou, China
3. State Key Laboratory of Marine Environmental Science, Xiamen University, Xiamen, China
4. Virginia Institute of Marine Science, Gloucester Point, VA, USA
5. Climate Simulations and Predictions Division, Centro Euro-Mediterraneo sui Cambiamenti Climatici (CMCC), Bologna, Italy

Correspondence to: Fei Chai (fchai@sio.org.cn) Yang Zhang (yzhang@sio.org.cn)

Abstract. As the demand for increased resolution and complexity in unstructured sea ice models is growing, a more advanced sea ice transport scheme is needed. In this study, we couple the Semi-implicit Cross-scale Hydro-science Integrated System Model (SCHISM) with Icepack, the column physics package of the sea ice model CICE; a key step is to implement a total variation diminishing (TVD) transport scheme for the multi-class sea ice module in the coupled model. Compared with the upwind scheme and a central difference scheme, the TVD transport scheme is found to have better performance for both idealized and realistic cases, and meets the requirements for conservation, accuracy, efficiency (even with very high resolution), and strict monotonicity. The coupled model for the Arctic Ocean successfully reproduces the long-term changes in the sea ice extent, the sea ice boundary and concentration observation from the satellite.

1 Introduction

The dramatically decrease in the Arctic Sea ice in recent decades due to global warming has a major impact on local and global climate (IPCC, 2019). In order to understand the changes in the physical and biogeochemical processes occurring in the Arctic Ocean, numerical models have become an important tool and they have been significantly improved in the past few decades. The sea ice, as a highly complex material (Hunke et al., 2020), received special attention, and the sea ice models have become more sophisticated in representing realistic physics. At present, an advanced sea ice model, the Los Alamos sea ice model (CICE, Hunke et al., 2015), including a stand-alone column physics package Icepack (Hunke et al., 2020), has incorporated multi-class thermodynamics, such as the Bitz and

https://doi.org/10.5194/gmd-2023-236
Preprint. Discussion started: 8 January 2024

Lipscomb (1999; BL99) thermodynamics formulation for constant salinity profiles, the mushy layer thermodynamics formulation for evolving salinity (Turner et al. 2013), and the sea ice ridging processes (Hunke, 2010). Many structured-grid models have been coupled with Icepack or CICE directly or via couplers, e.g., the Community Earth System Model (CESM, Hurrell et al.,2013) and the HYbrid Coordinate Ocean Model (HYCOM); others have partially incorporated and adapted CICE subroutines in their own ice module, e.g., the Sea Ice modelling Integrated Initiative (SI^3) of the Nucleus for European Modelling of the Ocean (NEMO, and NEMO can also couple with CICE or The Louvain-La-Neuve sea ice model, LIM3, Gurvan et al., 2022), and The Thermodynamic Sea Ice Package (THSICE) of the Massachusetts Institute of Technology General Circulation Model (MITgcm, Campin et al. 2023). For the unstructured-grid (UG) models, Gao et al. (2011) have incorporated the Unstructured-Grid CICE (UG-CICE) into the unstructured-grid Finite Volume Community Ocean Model (FVCOM, Chen et al., 2012). Some other unstructured-grid models have incorporated Icepack directly, e.g., the Finite-volumE Sea ice-Ocean Model version 2 (FESOM2, Danilov et al., 2017) and the Model for Prediction Across Scales (MPAS-Seaice, Turner et al., 2022). Note that when Icepack is incorporated into another model, the latter must also implement its own dynamic solver for momentum and transport. UG-CICE and FESOM2 use triangular mesh grids while MPAS-Seaice uses Voronoi dual graph. UG-CICE uses a finite-volume formulation, the sea ice component allows for five ice categories, four layers of ice and one layer of snow. The other models allow users to specify the number of categories. UG-CICE can produce good results on the seasonal variability of the sea ice in the Arctic Ocean (Gao et al., 2011). FESOM2 has implemented Icepack in its entirety and found that more complex model formulations lead to better results (Zampieri et al., 2021). MPAS-Seaice can be viewed as the unstructured version of CICE, and thus shares sophisticated thermodynamics and biogeochemistry with CICE, including BL99 and mushy layer, and is the current sea-ice component of the Energy Exascale Earth System Model (E3SM, Turner et al., 2022). A summary of these sea-ice models is given in Table 1.

Model	Ice model	Grid	Thermodynamic	Transport solver	Coupling method
CESM	CICE	Structured	BL99 Mushy Layer	Incremental remapping scheme/ Upwind scheme	Coupler
NEMO	CICE, LIM3, SI^3	Structured	Mushy Layer	Prather scheme/ ULTIMATE-MACHO scheme (SI^3)	Direct (with SI^3)
HYCOM	CICE	Structured	BL99 Mushy Layer	Incremental remapping scheme/ Upwind scheme	Coupler

https://doi.org/10.5194/gmd-2023-236
Preprint. Discussion started: 8 January 2024

MITgcm	THSICE	Structured	Two layers of ice and one layer of snow	2nd-order flux limited scheme	Direct
E3SM	MPAS-Seaice	Unstructured	BL99 Mushy Layer	Incremental remapping scheme/ Upwind scheme	Coupler
UG-CICE	CICE	Unstructured	Four layers of ice and one layer of snow	Second order upwind scheme	Direct
FESOM2	ICEPACK	Unstructured	BL99 Mushy Layer	FEM-FCT	Direct

Table 1. Comparison of several sea ice models

With the advancement in High Performance Computing, sea ice coupled models are increasingly executed on higher spatial and temporal resolutions. The increased demand for resolution and complexity in the sea ice models calls for an accurate, stable, conservative, strictly monotonic, and efficient sea ice transport method (Hunke et al. 2010). The sea ice transport method has been studied for many years, and various schemes have been proposed. Lipscomb et al. (2004) implemented the upwind and incremental remapping schemes in CICE, both of which are still available in the latest version. The upwind scheme is the simplest scheme for transport, but it is too diffusive due to its first order accuracy. The incremental remapping scheme is a second-order accurate scheme, and has great performance in structured grid models, but is inefficient for highly distorted UGs. For example, MPAS-Seaice uses the incremental remapping scheme (Turner et al., 2022), but as a global model, its resolution is usually coarse. MITgcm offers many tracer advection solvers, but it recommends flux-limited schemes to avoid unphysical results (Campin et al. 2023). NEMO uses the Prather scheme or the ULTIMATE-MACHO scheme with SI^3 ice model (Gurvan et al., 2022), both of which require some functions to limit the tracer concentrations from exceeding the largest values of all adjacent nodes. The efficiency has not been well tested on those SG models under very high resolution down to about tens of meters.

In the case of triangular UGs, the transport scheme utilized in UG-CICE is the second-order upstream scheme, which considers the gradient of sea ice tracers (Gao et al., 2011). This scheme is consistent with the tracer transport in FVCOM (Chen et al., 2012). It is unclear if the monotonicity is guaranteed by this scheme or if additional diffusion is needed. The transport scheme of FESOM2 is the Finite Element Flux Corrected Transport scheme (FEM-FCT, Löhner et al., 1987), which is based on the finite element description (Danilov et al. 2015). It is also a conservative and second-order scheme (Budgell, et al. 2007), but its cost is linearly increasing with the number of variables, and more importantly, strict monotonicity comes with a higher cost (Löhner et al., 1987). Therefore, Zhang et al. (2023) used the upwind scheme by zeroing out the higher-order contribution in their study with very high resolution.

SCHISM, which has the seamless cross-scale capability from creek to ocean (Zhang et al., 2016), has been applied to study the Great Lake ice formation process and obtained reasonable results in very high

https://doi.org/10.5194/gmd-2023-236
Preprint. Discussion started: 8 January 2024


Geoscientific Model Development Discussions

resolution (Zhang et al., 2023), using a single-class ice/snow module borrowed from FESOM (Danilov et al., 2015). The thermodynamics employed is a 0-layer thermodynamic module (Parkinson & Washington, 1979), with constant dry and melting albedos of ice and snow. In the simulation of The Great Lake ice formation process, both SCHISM and single-class ice model allow multi-scale physics on variable resolution (Zhang et al., 2023). However, the performance of the multi-class sea ice formulation has not been tested before. SCHISM therefore represents a mature and reliable platform to implement the multi-class sea ice module, Icepack.

This paper presents a new unstructured ice-ocean coupled model built on SCHISM and Icepack. The coupled model utilizes the TVD transport scheme to achieve an efficient, strictly monotone, second-order accuracy scheme for ice tracers on generic unstructured grids (even with locally very high resolution). Section 2 introduces components of the coupled model and describes how the TVD transport scheme is implemented for the ice model. In Section 3, we compare some ideal test results from the new TVD scheme with two other methods (the upwind scheme and a central difference scheme) and compare the efficiency with upwind scheme when applied to a high-resolution mesh; we also validate the new coupled model with a simulation of the Arctic Ocean sea ice with realistic atmosphere forcing. Section 4 compares the new TVD scheme with other TVD schemes. Section 5 summarizes the major findings of this work.

2 Method

2.1 Icepack implemented in SCHISM

We couple Icepack v1.3.4 (Hunke et al., 2023) with SCHISM v5.11. Besides the 0-layer thermodynamics, two more sophisticated thermodynamic formulations, BL99 and the mushy layer are also implemented. At the sub-grid scale, thin and thick ice coexist, and therefore an ice thickness distribution (ITD, Bitz et al.,2001) has been implemented in order to describe the unresolved spatial heterogeneity of the thickness field. The ITD provides a prognostic statistical description of the sea ice thickness partitioned into multiple categories and of the ice area fraction associated to each category, instead of only one fraction as in the previous implementation. More traces and more ice processes are added in this new version of Icepack, including multiple melt ponds parameterizations (Hunke et al., 2013) and a mechanical redistribution parameterization (Hunke 2010) that responds to sea ice convergence by piling up thin sea ice and therefore mimicking ridging and rafting events. The interaction

https://doi.org/10.5194/gmd-2023-236
Preprint. Discussion started: 8 January 2024

Geoscientific Model Development Discussions

between the shortwave radiation and the sea ice in Icepack is described by the 'Community Climate System Model (CCSM3)' formulation, which links the surface albedo to the surface sea ice temperature, or the Delta-Eddington formulation (Briegleb et al., 2007), which links the albedo to inherent optical properties of sea ice and snow. The dynamic solver is not included in Icepack and is based on two approaches: 1. a classic Elastic-Viscous-Plastic method (EVP, Hunke & Dukowicz, 1997), and 2. modified Elastic-Viscous-Plastic method (mEVP, Kimmritz et al., 2015), both inherited from the old single-class ice/snow formulation (Zhang et al. 2023). All ice-related subroutines are called at every ocean step by SCHISM's hydrodynamic core. The ice module exports to SCHISM variables needed for coupling such as the shortwave radiation, the ice-ocean heat flux, the freshwater flux, and finally the sea ice pressure and ice-ocean stress for all ice-covered nodes, in proportion to the sea ice area fraction. Over open ocean these variables are calculated directly by SCHISM. All variables required by Icepack can be obtained from either SCHISM or separate input files.

2.2 Schemes for sea ice transport

The basic transport equation of sea ice area or fraction a_n for each sea ice category is (Thorndike et al. 1975),

$$\frac{\partial a_n}{\partial t} + \frac{\partial u a_n}{\partial x} + \frac{\partial v a_n}{\partial y} + \frac{\partial}{\partial h}(a_n f) = \psi, \quad (1)$$

Where u and v are the ice velocities of x and y components, respectively, and h is the ice thickness. The last term on the left side is thermodynamic change, where f is the rate of ice melting or growing, and the right-side term ψ is mechanical redistribution like the ridging process. We solve this equation using a fractional step method: first solve a pure advection equation (i.e. by setting the thermodynamic term and mechanical redistribution term to 0), followed by a correction step that includes the remaining terms. The main challenge occurs in the first step, where we must solve a pure advection equation for one category of sea ice fraction a_n:

$$\frac{\partial a_n}{\partial t} + \frac{\partial u a_n}{\partial x} + \frac{\partial v a_n}{\partial y} = 0, \quad (2)$$

https://doi.org/10.5194/gmd-2023-236
Preprint. Discussion started: 8 January 2024

Geoscientific Model Development Discussions

Note that the ice velocity field is divergent, which can produce new local maxima/minima. However, a strictly monotone scheme is still desirable in order to separate the numerical dispersion from the physical convergence.

We apply a finite volume algorithm to discretize equation (2). Unlike the Arakawa-CD grid used in SCHISM, the sea ice module inside SCHISM employs an Arakawa-A grid, with both the sea ice velocity and traces located at the node (blue circles in Fig.1). The tracer control volume is defined as the polygon enclosed by the lines composed of centroids and edge centers (red circles in Fig.1). So, in the subsequent time step, after Δt, the new ice fraction is:

$$a_n^{t+1} = a_n^t + \frac{\Delta t \sum_{i \in S} Q_i \phi_i}{\Omega_S}, \tag{3}$$

Ω_S is the total area of the control volume; S is its boundary, and Q_i is the flux across the edge i of the control volume. Most of these variables can be obtained easily in the model, so we only focus on finding a method to proximate the edge tracer value, ϕ_i.

The simplest method is the first order upwind scheme (assuming, without loss of generality, the velocity direction is as depicted in Fig. 1):

$$\phi_i = \phi_C, \tag{4}$$

The central difference scheme is

$$\phi_i = \frac{1}{2}(\phi_C + \phi_D), \tag{5}$$

Where ϕ_C and ϕ_D are the values at the upwind and the downwind nodes, respectively, for one edge of the control volume (Fig.1a).

The TVD corrects the upwind values as:

$$\phi_i = \phi_C + \frac{\psi_i}{2}(\phi_D - \phi_C), \tag{6}$$

The last term on right side is the anti-diffusion correction. In this part, ψ_i is a function of the upwind ratio, r_i, for which we select the Van-leer limiter (van Leer, 1979),

$$\psi_i = \frac{r_{i*} + |r_i|}{1 + |r_i|}, \tag{7}$$

$$r_i = \frac{\phi_C - \phi_{U*}}{\phi_D - \phi_C}, \tag{8}$$

Where ϕ_{U*} is defined as the upwind node of the upwind node (i.e., ‘up-upwind’), and can be accessed easily in a structured grid or a uniform unstructured grid (Fig.1a). But for generic unstructured grids, how to approximate ϕ_{U*} is a key issue for the TVD scheme. There are several possible choices for ϕ_{U*}, and

https://doi.org/10.5194/gmd-2023-236
Preprint. Discussion started: 8 January 2024

Geoscientific Model Development Discussions
Open Access
EGU

after some comparisons we choose the method proposed by Darwish et al. (2003). This method includes the gradient of the central node $\nabla\phi_C$.

$$\phi_{U*} = \phi_D + R_{DU} \cdot (\nabla\phi_C) = \phi_D - 2R_{CD} \cdot (\nabla\phi_C), \quad (9)$$

where R_{DU} is the vector from the downwind node to the up-upwind node, and R_{CD} is the vector from the upwind to downwind nodes.

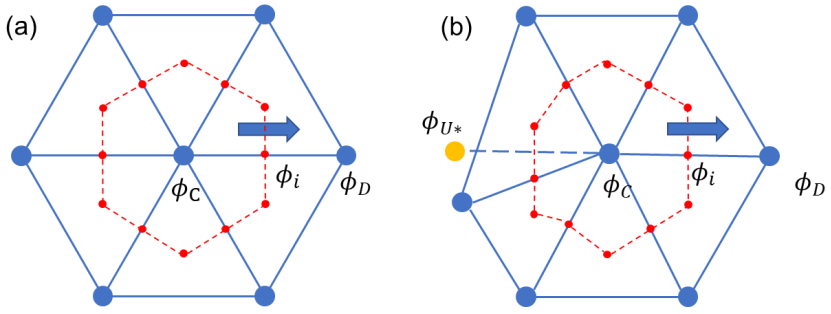

Figure 1. Schematics of control volume for the ice transport; **(a)** is for a uniform unstructured mesh, **(b)** is for a generic unstructured mesh.

As the sea ice concentration cannot exceed 1 or be negative in this pure advection step (but after the transport step, it can exceed 1 and lead to the ridging process, and in the latter case, Icepack will perform clipping), Darwish's method (9) can produce errors and needs to be limited:

$$\phi_{U*} = \min\left(1, max\left(0, \phi_D - 2R_{CD} \cdot (\nabla\phi_C)\right)\right), \quad (10)$$

Using the approximation of edge tracer values ϕ_{U*}, we can calculate the sea ice fluxes across every edge of the control volume, and thus the new concentration from Eq. (3). Other tracer fluxes like volume per unit area of ice and enthalpy depend on the area fluxes, as does CICE. For instance, the volume per unit area of ice v_n equals the product of the sea ice area a_n and the sea ice thickness h_n, here h_i is the sea ice thickness of the upwind node.

$$v_n = a_n h_n, \quad (11)$$

$$v_n^{t+1} = v_n^t + \frac{\Delta t \sum_{i\in S} Q_i \phi_i h_i}{\Omega_S}, \quad (12)$$

Sea ice enthalpy e_n is the product of the sea ice area a_n, the sea ice thickness h_n and the energy per unit volume q_n, here q_i is the energy per unit volume of upwind node.

$$e_n = a_n h_n q_n, \quad (13)$$

$$e_n^{t+1} = e_n^t + \frac{\Delta t \sum_{i\in S} Q_i \phi_i h_i q_i}{\Omega_S}, \quad (14)$$

https://doi.org/10.5194/gmd-2023-236
Preprint. Discussion started: 8 January 2024

Other tracers at the new step can be calculated this way.

The finite-volume method ensures global and local conservation of tracers. Given that all ice area fluxes are recorded, flux calculation within the same category of ice only needs to be done once, so the method is computationally efficient. Numerous tests have demonstrated that the TVD scheme provides second-order accuracy in smooth regions (Zhang et al., 2015), and guarantees strict monotonicity and a good accuracy. The limiter we chose is the widely used Van-leer limiter. Even though the accuracy of this limiter may be locally reduced to first order, it always maintains monotonicity as long as the time step used satisfies the stability condition, as demonstrated by Sweby (1984). Sea ice concentration may produce new extremes after the transport step due to convergence. However, it should never be negative; this is guaranteed because the method in Eq. (3) is essentially a weighted average method with non-negative weights.

3 Result

3.1 Idealized test case

Since the thermodynamic part and dynamic parts of this model are relatively mature and have been widely utilized in other models, in this study we focus on validating the new transport scheme. The comparison of a few transport schemes is carried out through an idealized ice transport experiment in a uniform unstructured mesh. The mesh grid consists entirely of equilateral triangles, with a side length of 200m for each triangle. As the initial condition, we placed a rectangular sheet of sea ice with dimensions of 5000m x 5000m on the left side of the mesh. The initial ice thickness is 1.5m, and it moves to the right along the x-axis at a speed of 1m/s. The time step is 1 second, which satisfies the Courant-Friedrichs-Lewy condition of TVD (Zhang et al., 2016). We run the idealized experiment for 24 hours, or 86400 steps. We select two other schemes for comparison, the first order upwind scheme and the central difference scheme (with proper limiting based on local max/min). The skill metrics include the accuracy, conservation, and monotonicity of the results.

3.1.1 Accuracy

Fig. 2 shows the snapshots and central profiles along the x-axis of the sea ice concentration taken every 3 hours, with the theoretical solution represented by the red rectangles. For clarity, only areas with a concentration greater than 15% are shown. Compared to other schemes, the upwind scheme is

https://doi.org/10.5194/gmd-2023-236
Preprint. Discussion started: 8 January 2024

Geoscientific Model Development Discussions

significantly more diffusive, yet relatively uniform. The outline varies in shape, transitioning from a square to a circle. At the end of the model run, the peak of ice concentration is approximately 30% of the initial value, which is unsurprisingly the lowest among the three schemes. The central difference scheme retains more sea ice in the red rectangle than the upwind scheme. However, it produces non-uniform results even though the ice speed is uniform, and it requires clipping of under/overshoots (which violates the conservation). Some sea ice is left behind, with a banded distribution along the *x*-axis (Fig. 2b). The profiles portrayed in Fig. 2e indicate that the sea ice concentration exhibits multiple peaks while the peak ice concentration reaches approximately 90% in the end. Figs. 2c and 2f demonstrate that the TVD scheme has the best accuracy compared to the other two schemes. The horizontal distribution of the ice is closest to the analytical solution and exhibits a peak ice concentration around 100% at all times, despite some minor diffusion on the frontal edges.

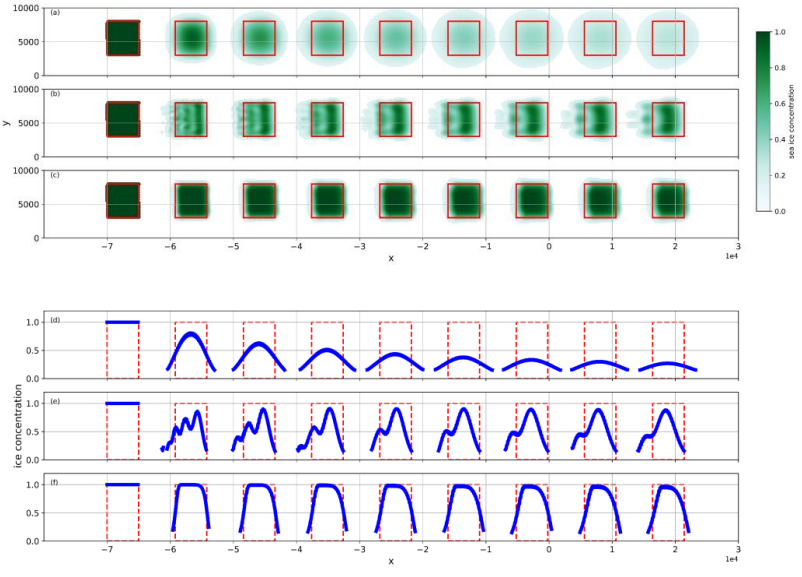

Figure 2. Sea ice concentration snapshots **(a-c)** and profiles **(d-f).** The sea ice moves from left to right, snapshots are taken every 3 hours, and the red rectangular is the exact solution**. (a, d)** Upwind, **(b, e)** Central difference, **(c, f)** TVD.

The results of the ice volume per unit area are similar to the ice concentration (Fig. 3). The upwind scheme is the most diffusive one. The peak of ice volume per unit area is only 0.4 meters at the end. The central difference scheme is superior to the upwind scheme, and there is no excessive amount of ice that lies outside the red rectangle on the top, bottom, and front edges. However, the scheme still shows

https://doi.org/10.5194/gmd-2023-236
Preprint. Discussion started: 8 January 2024

multiple peaks in Fig. 3e. Furthermore, it has obvious overshooting in all snapshots, which can be attributed to some spurious convergence processes that should not have occurred. The TVD scheme is the best of the three schemes. It performs well in terms of both shape and peak value. The shape of the ice volume per unit area is close to the theoretical solution from start to finish, with the peak value slightly (1.496m) lower than the exact result at the end. The ice volume from the upwind and TVD (Fig. 3d and f) has similar shapes to the ice concentration (Fig. 2d and f), indicating that both schemes maintain the monotonicity well, and we will discuss more on this later.

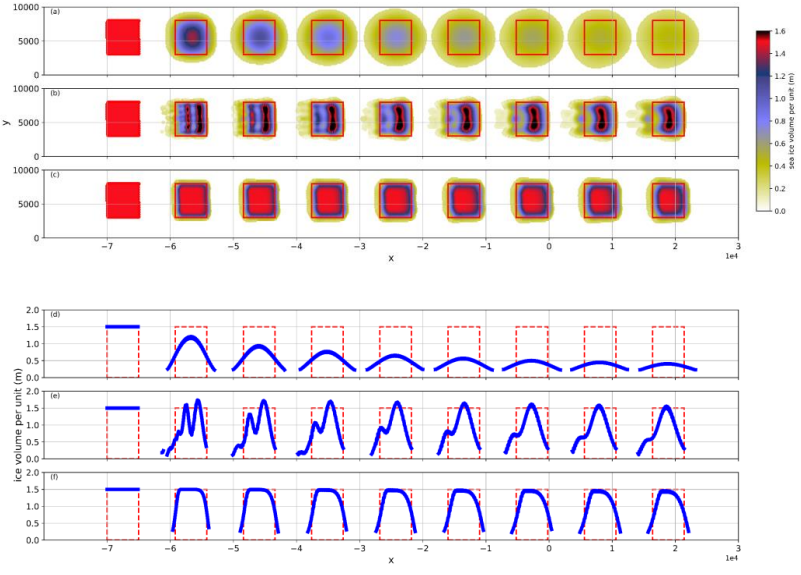

Figure 3. Volume per unit area of ice, with snapshots **(a-c)** and profiles **(d-f).** The sea ice moves from left to right, snapshots are taken every 3 hours, and the red rectangular is the exact solution. **(a, d)** Upwind, **(b, e)** Central difference, **(c, f)** TVD

3.1.2 Conservation

We assess the conservation property of schemes using two parameters to determine whether there is a loss or increase in sea ice area during transport. The first parameter is the ratio of the total ice area after transport to the initial total ice area. The second parameter is the ratio of the ice area that reaches the target area to the theoretical solution, which also indicates the degree of accuracy. In Table 2 we can see that, for the total area of ice, there is no change in area during the transport process using the upwind and TVD schemes. In contrast, the ice area of the central difference scheme declines initially, and then

https://doi.org/10.5194/gmd-2023-236
Preprint. Discussion started: 8 January 2024

increases over time. This suggests that the limiting procedure used in the central difference scheme destroys conservation. The upwind scheme performs relatively well at first, with ~72.34% ice reaching the target area after 1 hour. But its performance drops significantly, to ~25.76% at the end. The central difference scheme, achieves a percentage of ~60.29% at first, and at the end it manages to achieve ~55.11%. Among the three schemes, TVD is the most effective with a consistently higher percentage compared to the others. The percentage of the region reaching the target area exceeds 90% after 1 hour and consistently maintains a rate of nearly 80% towards the end.

		1 hour	3 hours	6 hours	12 hours	24 hours
Upwind	All area	100.00%	100%	100%	100%	100%
	In the target area	79.41%	65.71%	53.62%	39.40%	25.76%
Central difference	All area	72.34%	77.85%	80.92%	85.50%	91.82%
	In the target area	60.29%	59.08%	58.88%	57.08%	55.11%
TVD	All area	100.00%	100%	100%	100%	100%
	In the target area	91.23%	88.12%	85.67%	83.14%	79.22%

Table2. Ice area as a percentage of the exact solution.

3.1.3 Monotonicity

Here we select the ice thickness as the representative of traces to verify monotonicity, with the ideal transport scheme expected to maintain the initial ice thickness (1.5m). Fig.2e and Fig.3e have shown the central difference is not monotone as the ice thickness per unit area exceeds the initial maximum even in the first snapshot (3 hours after the start of the case); so we exclude it in the current comparison. Given that the non-monotonicity usually happens at low concentration areas, we choose 0.1% as the threshold. The upwind scheme is completely monotone and the ice thickness remains consistent with the initial value (Fig. 4a). For the TVD scheme, some overshoots would occur in the forward edge of ice (Fig.4b) if we did not limit the up-upwind value (cf. Eq. 9). On the other hand, the new TVD scheme we developed that limits the up-upwind value (cf. Eq. (10)) is completely monotone (Fig. 4c).

https://doi.org/10.5194/gmd-2023-236
Preprint. Discussion started: 8 January 2024

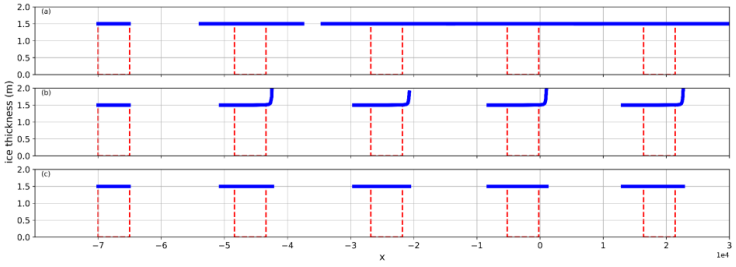

Figure 4. Sea ice thickness calculated from **(a)** Upwind, **(b)** original TVD (Eq. (9)), **(c)** new TVD (Eq. (10)) for ice. The time interval of snapshots is every 6 hours.

3.2 Realistic model run

A realistic ocean-ice coupled model using the TVD scheme for the ice module is developed to reproduce the ice processes in Lake Superior and the Arctic Ocean. In contrast to the idealized case, both meshes are non-uniform (Fig.5), so the successful tests demonstrate the cross-scale capability of the coupled model.

3.2.1 Test on a very high-resolution mesh

To gauge the numerical efficiency of the new TVD scheme, we test it on a very fine resolution Lake Superior mesh (Fig.5a) that was previously used in Zhang et al. (2023). The nearshore resolution in this mesh reaches ~50m with the finest resolution of 41.5m, found on the southwestern shore. As Zhang et al. (2023) indicated, the FCT scheme was having stability issues, so an essentially upwind method was applied in the high-resolution areas. The performance is compared with the upwind scheme. We simulate the case for 180 days from December 1st, 2017, using 48 processors. The total simulation times are similar with 2 schemes, 637 minutes for the TVD scheme and 654 minutes for the upwind. Note that the upwind scheme would be cheaper, but the total times shown include other modules in the model; the diffusion in the upwind scheme has led to a larger ice coverage area, thus increasing the cost of the ice solver. Overall, we found the cost for the TVD scheme is comparable to the upwind scheme for many realistic applications.

https://doi.org/10.5194/gmd-2023-236
Preprint. Discussion started: 8 January 2024

Geoscientific Model Development Discussions
Open Access
EGU

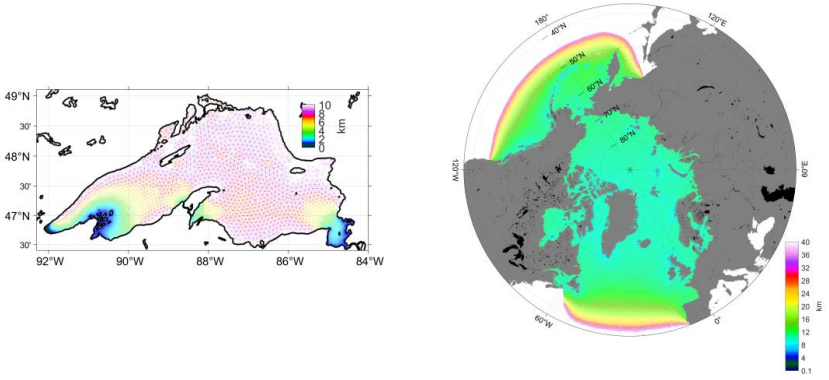

Figure 5. (a, left) The Lake Superior mesh. **(b, right)** The Arctic Ocean mesh. The colors show the mesh resolution.

Next, we qualitatively compare results from the two schemes on Day 100 (Fig.6), when the ice cover is largest. Results of ice concentration are similar, with higher concentration in the nearshore area and lower concentration in the center of the lake, which is consistent with the single-class ice model of Zhang et al. (2023). The TVD results reveal more variability especially in the open water. The results for the ice thickness are quite different, with thick ice further from the coast from the upwind result than from the TVD scheme (Fig. 6). This is because the upwind scheme is more diffusive than TVD. In the very high-resolution areas (southwestern and southeastern corners), both schemes yield reasonable and stable results, which demonstrates the coupled model's cross-scale capability.

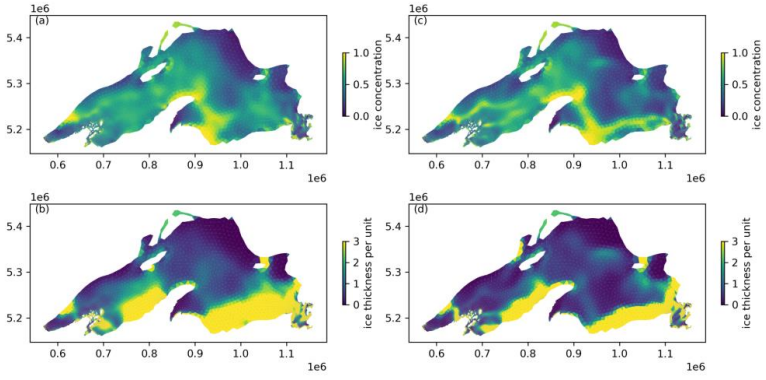

Figure 6. The top row is the ice concentration at Day 100, and **(a)** is the result of the upwind scheme **(c)** is that of the TVD scheme. The bottom row is the ice thickness per unit and **(b)** is for upwind, **(d) is** for TVD.

https://doi.org/10.5194/gmd-2023-236
Preprint. Discussion started: 8 January 2024


Geoscientific Model Development Discussions

315 **3.2.2 Test on the Arctic Ocean**

The Arctic mesh consists of 422,000 elements and 217,000 nodes (Fig. 5b) with the resolution ranging from 6 km near the coast to 40 km at the open boundary. The model starts on January 1st, 1994, and covers 2000 days, about 1.6 million steps using a time step of 100 sec. The initial condition is obtained from HYCOM, including ocean tracers, sea ice concentration and thickness. Moreover, the boundary
320 condition is obtained from HYCOM and Finite Element Solution (FES2014, Lyard et al., 2021), including 15 tidal components. The domain boundary is chosen to be at ~40°N to ensure no sea ice crosses the boundary. In the vertical dimension, a highly flexible vertical gridding system (LSC^2, Zhang et al., 2015) has been implemented with up to 60 layers in order to describe the complex topography of the Arctic Basin better, and we set the bottom drag coefficient with a constant manning
325 coefficient at 0.025. For the atmosphere forcing we choose The European Centre for Medium-Range Weather Forecasts Reanalysis Fifth Generation global reanalysis (ERA5, Hersbach et al., 2020) for its high temporal resolution, and use the bulk aerodynamic model (Zeng et al., 1998) to get the surface fluxes, like latent and sensible fluxes. The turbulence closure scheme in the hydro model is the generic length-scale equation as k-kl (Umlauf and Burchard, 2003) and the horizontal transport in the hydro
330 model is TVD^2 (Ye et al. 2016). The parameters used in the sea ice model basically follow the standard CICE configuration, including a constant air-ice drag coefficient (about 0.0016), and a constant ice-ocean drag coefficient (about 0.006). Modules in the standard CICE are also included in this model, e.g., the mushy layer thermodynamics, the Rothrock (1975) ice strength method, the level-ice melt ponds module, etc. We compare the results of our Arctic sea ice model with the NSIDC observation,
335 including the sea ice extent, ice boundary, and ice concentration. The observation of Sea Ice Concentrations is from Nimbus-7 SMMR and DMSP SSM/I-SSMIS Passive Microwave Data (Fetterer et al., 2017), while the sea ice boundary corresponds to the 15% sea-ice concentration contour. Fig.7a compares the sea ice extent of our model with the observation. The model is stable for the long-term test and has good performance to reproduce the inter-annual variability and the seasonal cycle,
340 with the minimum and maximum being reproduced satisfactorily. The first peak is higher than the observed value, which may be influenced by the initial conditions as we did not get all tracers, such as sea ice salinity and enthalpy, from HYCOM. The extent difference between the model and observation is evaluated as absolute extent error (AEE, Eq. 15). However, AEE may underestimate the model error

https://doi.org/10.5194/gmd-2023-236
Preprint. Discussion started: 8 January 2024

Geoscientific Model Development Discussions

due to the cancellation between the overestimation(O) and underestimation(U). The Integrated Ice Edge Error (IIEE, Eq. 16) may be a preferable choice to evaluate the simulation result (Goessling et al., 2016, Zampieri et al., 2018).

$$AEE = |\sum(|O| - |U|)|, \quad (15)$$

$$IIEE = \sum|O| + \sum|U|, \quad (16)$$

We present the monthly AEE and IIEE in Fig. 7b, provide monthly statistics for them and compare our results with the FESOM2's in Fig. 7c. FESOM2 team has run multiple cases to investigate the sensitive of results to various forcing and model complexities, and the ones we selected were also driven by ERA5 and based on a multi-class ice thermodynamics BL99 (Zampieri et al., 2021). IIEE and AEE (Fig. 7b) fluctuate in a similar fashion to the monthly extent in Fig.7a. In Fig.7a, the simulated sea ice extent often increases faster in autumn than observation, and it seems to perform better in other seasons. AEE shows a similar pattern, being relatively small in spring and summer, and reaching its maximum in autumn. The magnitude of AEE is also similar to that of FESOM2, peaking in autumn while lower in other seasons. The seasonal pattern of IIEE is similar to that of FESOM2, with maximum values during summer and lower values during autumn. The largest variability of IIEE occurs in summer, too, while the lowest variability is observed in spring. The differences between our model and FESOM2 may be caused by two factors. The first is that the results we select to compare from FESOM2 use different thermodynamic module and the second is that the integration period of FESOM2 is from 2002 to 2015, while this study's integration period is from 1994 to 1999. Nonetheless, the performance of the two models seems generally comparable.

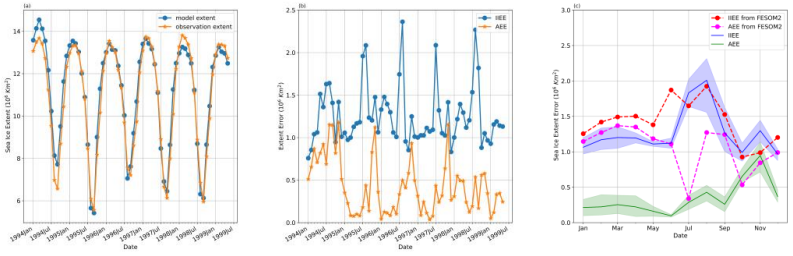

Figure 7. (a) Monthly sea ice extent of model and observation in the Arctic Ocean. **(b)** Monthly Integrated Ice Edge Error (IIEE) and Absolute Extent Error (AEE). **(c)** Monthly IIEE and AEE of our model and FESOM2 (averaged across all years), with the shading representing the 95% confidence intervals.

The comparison of the spatial sea ice concentration is shown in Fig.8. The simulated sea ice boundary and ice concentration show good agreement with the observation, and the model shows a robust ability

https://doi.org/10.5194/gmd-2023-236
Preprint. Discussion started: 8 January 2024

370 to capture the seasonal evolution of sea ice in the Arctic Ocean. During winter and spring (Fig. 8a and 8b), the deviation occurs in the marginal ice zone, such as the Bering Sea and the Atlantic Ocean. In summer (Fig.8c), the model overestimates the sea ice concentration near the coast, such as the Canadian archipelago coast, but underestimates in the central Arctic Basin. The overestimation is likely due to the presence of complex thermodynamic and dynamic processes in the coastal margin (e.g., the
375 occurrence of landfast sea ice). Furthermore, the lack of precise runoff and temperature data of Arctic rivers has a significant impact on the coastal area simulation. In the central Arctic Basin, melt ponds have a significant effect on the mass of sea ice during the melting season, and they are always formed as a certain amount of precipitation remains on the ice (Feng et al., 2022). The precipitation field we utilized shows some overestimation compared to the observation-based precipitation products
380 (Marcovecchio et al., 2021), so the underestimation of sea ice concentration in the central Arctic Basin is likely due to the excessive melt ponds that were reproduced in our model. In autumn (Fig.8d), the model overestimates sea ice concentration in the marginal seas of the Arctic, like Hudson and Baffin Bay, which causes the largest AEE. The heat exchange between the air-ice-sea interface is generally more intense in the freezing season than melting season, so the coupled model may generate more sea
385 ice due to its inability to deliver sufficient heat to the surface in time or due to the insufficient strength of convection in the upper ocean.

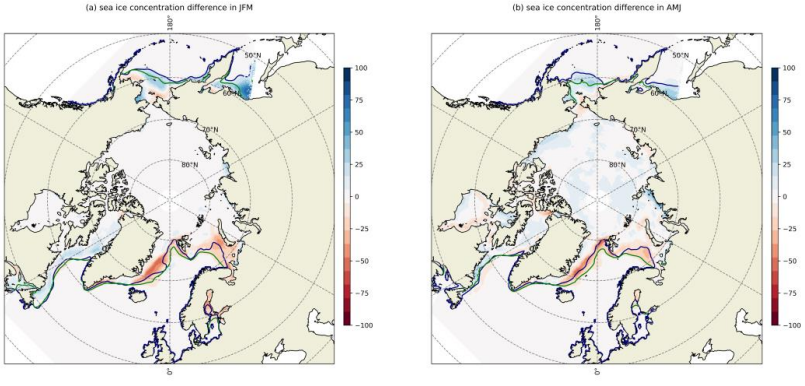

https://doi.org/10.5194/gmd-2023-236
Preprint. Discussion started: 8 January 2024

Geoscientific Model Development Discussions
Open Access
EGU

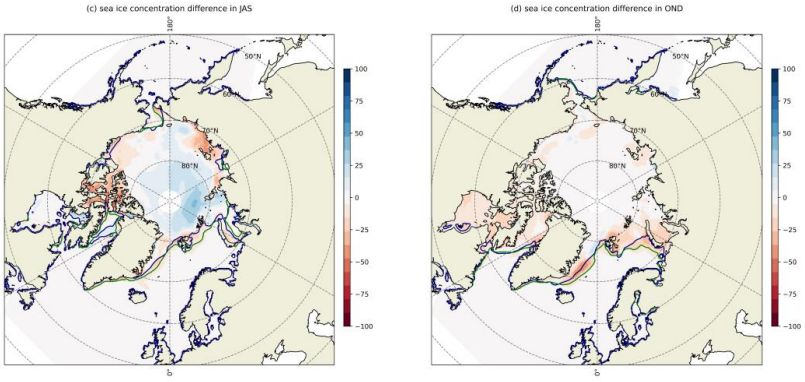

Figure 8. Seasonally averaged sea ice concentration difference (Observation-Model). The blue line is the satellite sea ice boundary, and the green line is from the model. **(a)** Winter (Jan. Feb. and Mar.), **(b)** Spring (Apr. May. and Jun.), **(c)** Summer (Jul. Aug. and Sept.), **(d)** Autumn (Oct. Nov. and Dec.)

4 Discussion

In this study, the grid definition is different between the ice module and the hydrodynamic module. The ice module uses the Arakawa-A grid, and all tracers and velocities are defined at nodes, while the hydrodynamic module uses the Arakawa-CD grid. The main reason behind this decision is that we adapted the rheology part from FESIM, which uses an analogue of the Arakawa-A grid, and it performs well for sea ice simulation while saving computational costs (Danilov et al., 2015). For a coarse mesh, the Arakawa-A grid delivers performance similar to that of the Arakawa-CD grid in simulating sea ice deformations (Mehlmann et al., 2021). In a pure advection case, the oscillations are weaker for the Arakawa-A grid with tracers located at the node, compared to the case with the tracers located at the centroid (Zhang et al., 2016). The coupling between the ice module and the hydrodynamic module remains unaffected by the differences in the variable definition, as all forcing variables are located at nodes in the hydrodynamic module. Under the uniform mesh in the idealized test, the central difference scheme is similar to the second order upstream scheme of UG-CICE, and the latter achieved remarkable results (Gao et al., 2013). The difference in stencils used between UG-CICE and this work may explain why the central difference scheme has an unsatisfactory performance: in UG-CICE, tracers are also at vertices (nodes) but the velocity is at the centroids. Still, it remains unclear if UG-CICE is strictly monotone.

https://doi.org/10.5194/gmd-2023-236
Preprint. Discussion started: 8 January 2024


Geoscientific Model Development Discussions

The TVD scheme used in this work is based on the gradient of the central node, whereas Casulli et al. (2005) used the flux into the element to obtain the ϕ_{U*} in order to avoid unphysical overshoots/undershoots. For the Casulli's TVD scheme, the tracers are always located at the centroid, but they also can be converted to the node (Zhang et al., 2016). A comparison of the results for the idealized cases from Casulli's TVD and our TVD scheme revealed that Casulli's TVD scheme has more diffusion than the new TVD scheme.

5 Conclusion

We have incorporated a multi-class sea ice module, the advanced sea ice column physics package Icepack, into the SCHISM modelling system. Significantly, we have implemented a new TVD based scheme for ice tracer transport and validated it using an idealized case and realistic cases. The simulation results demonstrate that the TVD scheme is conservative, accurate, strictly monotonic, and efficient in reproducing the horizontal transport of ice and has better performance than the upwind and central schemes. The coupled model for the Arctic Ocean was able to reproduce the Arctic Sea ice concentration, boundary, and extent as seen from the observation.

An advantage of the coupled SCHISM-Icepack is its ability to effectively simulate ocean-ice evolution in both open ocean and coastal regions. In addition, SCHISM includes various biogeochemistry modules like CoSiNE, while Icepack contains a biogeochemistry module as well. We will further investigate the under-ice ecosystem changes caused by global warming by integrating those biogeochemistry modules.

Code and data availability.

Code of this model have two components, Icepack 1.3.4 and SCHISM v5.11. Icepack 1.3.4 is obtained from https://github.com/CICE-Consortium/Icepack . SCHISM v5.11 and the coupled model can be found at https://github.com/schism-dev/schism, including all the code used in this paper. All source code is also available on Zenodo (https://doi.org/10.5281/zenodo.10391035, Wang et al., 2023) with all configuration files of the idealized case and the realistic test on the Arctic Ocean. In the realistic test on the Arctic Ocean, the forcing data is from ERA5, initial and boundary data is from HYCOM and

https://doi.org/10.5194/gmd-2023-236
Preprint. Discussion started: 8 January 2024

FES2014, they can be generated by the preprocessing script in SCHISM. The input data of the realistic case on the Lake Superior is available from Y. Joseph Zhang on reasonable request. All the results in the paper are also available from Qian Wang on reasonable request.

Author contributions

Qian Wang: Data curation, Formal analysis, Investigation, Methodology, Software, Visualization, Writing – original draft preparation. **Fei Chai**: Conceptualization, Supervision, Funding acquisition, Project administration. **Yang Zhang**: Validation, Resources, Software, Writing – review & editing. **Y. Joseph Zhang**: Validation, Methodology, Software, Writing – review & editing. **Lorenzo Zamperi**: Writing – review & editing.

Competing interests

The authors declare that they have no conflict of interest.

Acknowledgements

The authors acknowledge the financial support of the National Natural Science Foundation of China (Grant Number 41941013). The study in this paper was supported by the high-performance computing clusters at: (1) State Key Laboratory of Satellite Ocean Environment Dynamics, SIO, MNR; (2) William & Mary Research Computing (URL: https://www.wm.edu/it/rc). The authors also thank HYCOM data server for their sea ice product. Lorenzo Zampieri acknowledges the financial support of the Italian National Recovery and Resilience Plan (PNRR) through the "SPOKE 4 - EARTH & CLIMATE" program.

Financial support

This work is supported by the National Natural Science Foundation of China (Grant Number 41941013)

References

Bitz, C. M., Holland, M. M., Weaver, A. J., & Eby, M. Simulating the ice-thickness distribution in a coupled climate model. Journal of Geophysical Research: Oceans, 106(C2), 2441-2463, https://doi.org/10.1029/1999JC000113, 2001.

https://doi.org/10.5194/gmd-2023-236
Preprint. Discussion started: 8 January 2024

Bitz, C. M. and Lipscomb, W. H.: An energy-conserving thermodynamic model of sea ice, J. Geophys. Res.-Oceans, 104, 15669–15677, https://doi.org/10.1029/1999JC900100, 1999.

Briegleb, B. P. and Light, B.: A Delta-Eddington multiple scattering parameterization for solar radiation in the sea ice component of the Community Climate System Model, Tech. Rep. NCAR/TN 472+STR, National Center for Atmospheric Research, Boulder, Colorado USA, https://doi.org/10.5065/D6B27S71, 2007.

Budgell, W. P., Oliveira, A., and Skogen, M. D.: Scalar advection schemes for ocean modelling on unstructured triangular grids, Ocean Dynamics, 57, 339-361, https://doi.org/10.1007/s10236-007-0111-8, 2007.

Casulli, V. and Zanolli, P.: High resolution methods for multidimensional advection–diffusion problems in free-surface hydrodynamics, Ocean Modelling, 10, 137-151, https://doi.org/10.1016/j.ocemod.2004.06.007, 2005.

Chen, C., Beardsley, R. C., Cowles, G., Qi, J., Lai, Z., Gao, G., ... & Lin, H. An unstructured-grid, finite-volume community ocean model: FVCOM user manual. Cambridge, MA, USA: Sea Grant College Program, Massachusetts Institute of Technology. 2012.

Danilov, S., Sidorenko, D., Wang, Q., and Jung, T.: The Finite-volumE Sea ice–Ocean Model (FESOM2), Geoscientific Model Development, 10, 765-789, https://doi.org/10.5194/gmd-10-765-2017, 2017.

Danilov, S., Wang, Q., Timmermann, R., Iakovlev, N., Sidorenko, D., Kimmritz, M., Jung, T., and Schröter, J.: Finite-Element Sea Ice Model (FESIM), version 2, Geoscientific Model Development, 8, 1747-1761, https://doi.org/10.5194/gmd-8-1747-2015, 2015.

Darwish, M. S., & Moukalled, F. TVD schemes for unstructured grids. International Journal of heat and mass transfer, 46(4), 599-611. https://doi.org/10.1016/S0017-9310(02)00330-7, 2003.

Elizabeth Hunke, Richard Allard, David A. Bailey, Philippe Blain, Anthony Craig, Frederic Dupont, Alice DuVivier, Robert Grumbine, David Hebert, Marika Holland, Nicole Jeffery, Jean-Francois Lemieux, Robert Osinski, Till Rasmussen, Mads Ribergaard, Lettie Roach, Andrew Roberts, Matthew Turner, & Michael Winton. CICE-Consortium/Icepack: Icepack 1.3.4 (1.3.4). Zenodo. https://doi.org/10.5281/zenodo.8336034, 2023.

Feng, J., Zhang, Y., Cheng, Q., and Tsou, J. Y.: Pan-Arctic melt pond fraction trend, variability, and contribution to sea ice changes, Global and Planetary Change, 217, https://doi.org/10.1016/j.gloplacha.2022.103932, 2022.

https://doi.org/10.5194/gmd-2023-236
Preprint. Discussion started: 8 January 2024

Fetterer, F., K. Knowles, W. N. Meier, M. Savoie, and A. K. Windnagel.. Sea Ice Index, Version 3 [Data Set]. Boulder, Colorado USA. National Snow and Ice Data Center. https://doi.org/10.7265/N5K072F8. Date Accessed 08-05-2023. 2017.

Gao, G., Chen, C., Qi, J., and Beardsley, R. C.: An unstructured-grid, finite-volume sea ice model: Development, validation, and application, Journal of Geophysical Research, 116, https://doi.org/10.1029/2010JC006688, 2011.

Goessling, H. F., Tietsche, S., Day, J. J., Hawkins, E., and Jung, T.: Predictability of the Arctic sea ice edge, Geophysical Research Letters, 43, 1642-1650, https://doi.org/10.1002/2015GL067232, 2016.

Hersbach, H., Bell, B., Berrisford, P., Hirahara, S., Horányi, A., Muñoz-Sabater, J., ... & Thépaut, J. N. The ERA5 global reanalysis. Quarterly Journal of the Royal Meteorological Society, 146(730), 1999-2049. https://doi.org/10.1002/qj.3803, 2020.

Hunke, E. C. Thickness sensitivities in the CICE sea ice model. Ocean Modelling, 34(3-4), 137-149. https://doi.org/10.1016/j.ocemod.2010.05.004, 2010.

Hunke, E., Allard, R., Blain, P., Blockley, E., Feltham, D., Fichefet, T., Garric, G., Grumbine, R., Lemieux, J. F., Rasmussen, T., Ribergaard, M., Roberts, A., Schweiger, A., Tietsche, S., Tremblay, B., Vancoppenolle, M., and Zhang, J.: Should Sea-Ice Modeling Tools Designed for Climate Research Be Used for Short-Term Forecasting?, Curr Clim Change Rep, 6, 121-136, https://doi.org/10.1007/s40641-020-00162-y, 2020.

Hunke, E. C. and Dukowicz, J. K.: An elasticviscous-plastic model for sea ice dynamics, J. Phys. Oceanogr., 27, 1849–1867, https://doi.org/10.1175/1520-0485(1997)027<1849:AEVPMF>2.0.CO;2, 1997.

Hunke, E. C., Hebert, D. A., & Lecomte, O. Level-ice melt ponds in the Los Alamos sea ice model, CICE. Ocean Modelling, 71, 26-42. https://doi.org/10.1016/j.ocemod.2012.11.008, 2013

Hunke, E. C., Lipscomb, W. H., Turner, A. K., Jeffery, N., and Elliott, S.: CICE: the Los Alamos sea ice model documentation and software user's manual version 5.1, Tech. Rep., Los Alamos National Laboratory, LA-CC-06-012, https://github.com/CICE-Consortium/CICE-svn-trunk/blob/main/cicedoc/cicedoc.pdf (last access: 4 April 2022), 2015.

Hunke, E. C., Lipscomb, W. H., & Turner, A. K. Sea-ice models for climate study: retrospective and new directions. Journal of Glaciology, 56(200), 1162-1172. https://doi.org/10.3189/002214311796406095, 2010.

https://doi.org/10.5194/gmd-2023-236
Preprint. Discussion started: 8 January 2024

Hurrell, J. W., Holland, M. M., Gent, P. R., Ghan, S., Kay, J. E., Kushner, P. J., ... & Marshall, S. The community earth system model: a framework for collaborative research. Bulletin of the American Meteorological Society, 94(9), 1339-1360. https://doi.org/10.1175/BAMS-D-12-00121.1, 2013.

Jean-Michel Campin, Patrick Heimbach, Martin Losch, Gael Forget, edhill3, Alistair Adcroft, amolod, Dimitris Menemenlis, dfer22, Oliver Jahn, Chris Hill, Jeff Scott, stephdut, Matt Mazloff, Baylor Fox-Kemper, antnguyen13, Ed Doddridge, Ian Fenty, Michael Bates, Timothy Smith, AndrewEichmann-NOAA, mitllheisey, Jonathan Lauderdale, Torge Martin, Ryan Abernathey, Ou Wang, samarkhatiwala, dngoldberg, hongandyanand Bruno Deremble: MITgcm/MITgcm: ckeckpoint68r, https://doi.org/10.5281/zenodo.8208482, 2 August 2023.

Kimmritz, M., Danilov, S., and Losch, M.: On the convergence of the modified elastic-viscous-plastic method for solving the sea ice momentum equation, J. Comput. Phys., 296, 90–100, https://doi.org/10.1016/j.jcp.2015.04.051, 2015.

Lipscomb, W. H. and Hunke, E. C.: Modeling sea ice transport using incremental remapping, Mon. Weather Rev., 132, 1341–1354, https://doi.org/10.1175/1520-0493(2004)132<1341:MSITUI>2.0.CO;2, 2004.

Löhner, R., Morgan, K., Peraire, J., & Vahdati, M. Finite element flux-corrected transport (FEM–FCT) for the euler and Navier–Stokes equations. International Journal for Numerical Methods in Fluids, 7(10), 1093-1109. https://doi.org/10.1002/fld.1650071007, 1987.

Lyard, F. H., Allain, D. J., Cancet, M., Carrère, L., & Picot, N.. FES2014 global ocean tide atlas: design and performance. Ocean Science, 17(3), 615-649. https://doi.org/10.5194/os-17-615-2021, 2021.

Madec Gurvan, Romain Bourdallé-Badie, Jérôme Chanut, Emanuela Clementi, Andrew Coward, Christian Ethé, Doroteaciro Iovino, Dan Lea, Claire Lévy, Tomas Lovato, Nicolas Martin, Sébastien Masson, Silvia Mocavero, Clément Rousset, Dave Storkey, Simon Müeller, George Nurser, Mike Bell, Guillaume Samson, Pierre Mathiot, Francesca Meleand Aimie Moulin: NEMO ocean engine, https://doi.org/10.5281/zenodo.6334656, 7 March 2022.

Marcovecchio, A., Behrangi, A., Dong, X., Xi, B., and Huang, Y.: Precipitation influence on and response to early and late Arctic sea ice melt onset during melt season, International Journal of Climatology, 42, 81-96, https://doi.org/10.1002/joc.7233, 2021.

Mehlmann, C., Danilov, S., Losch, M., Lemieux, J. F., Hutter, N., Richter, T., Blain, P., Hunke, E. C., and Korn, P.: Simulating Linear Kinematic Features in Viscous-Plastic Sea Ice Models on Quadrilateral

and Triangular Grids With Different Variable Staggering, Journal of Advances in Modeling Earth Systems, 13, https://doi.org/10.1029/2021MS002523, 2021.

Meredith, M., Sommerkorn, M., Cassota, S., Derksen, C., Ekaykin, A., Hollowed, A., Kofinas, G., Mackintosh, A., Melbourne-Thomas, J., Muelbert, M., Ottersen, G., Pritchard, H., Schuur, E., Boyd, P., Hobbs, W. and Hodgson-Johnston, I.: Polar Regions, https://hdl.handle.net/102.100.100/516805, 2019.

Parkinson, C. L. and Washington, W. M.: A large-scale numerical model of sea ice, J. Geophys. Res., 84, 311–337, https://doi.org/10.1029/JC084iC01p00311, 1979.

Rothrock, D. A.: The energetics of the plastic deformation of pack ice by ridging, Journal of Geophysical Research, 80, 4514-4519, https://doi.org/10.1029/JC080i033p04514, 1975.

Sweby, P. K. High resolution schemes using flux limiters for hyperbolic conservation laws. SIAM journal on numerical analysis, 21(5), 995-1011. https://doi.org/10.1137/0721062, 1984.

Thorndike, A. S., Rothrock, D. A., Maykut, G. A., and Colony, R., The thickness distribution of sea ice, J. Geophys. Res., 80(33), 4501–4513, https://doi.org/10.1029/JC080i033p04501, 1975.

Turner, A. K., Hunke, E. C., and Bitz, C. M.: Two modes of sea-ice gravity drainage: A parameterization for largescale modeling, J. Geophys. Res.-Oceans, 118, 2279–2294, https://doi.org/10.1002/jgrc.20171, 2013.

Turner, A. K., Lipscomb, W. H., Hunke, E. C., Jacobsen, D. W., Jeffery, N., Engwirda, D., Ringler, T. D., and Wolfe, J. D.: MPAS-Seaice (v1.0.0): sea-ice dynamics on unstructured Voronoi meshes, Geoscientific Model Development, 15, 3721-3751, https://doi.org/10.5194/gmd-15-3721-2022, 2022.

Umlauf, L., & Burchard, H. A generic length-scale equation for geophysical turbulence models. Journal of Marine Research, 61(2), 235-265. http://dx.doi.org/10.1357/002224003322005087 2003.

Van Leer, B. Towards the ultimate conservative difference scheme. V. A second-order sequel to Godunov's method. Journal of computational Physics, 32(1), 101-136. https://doi.org/10.1016/0021-9991(79)90145-1, 1979.

Wang, Q., Chai, F., Zhang, Y., Zhang, J. Y., & Zamperi, L. Dataset of 'Development of a total variation diminishing (TVD) Sea ice transport scheme and its application in in an ocean (SCHISM v5.11) and sea ice (Icepack v1.3.4) coupled model on unstructured grids' [Data set]. Zenodo. https://doi.org/10.5281/zenodo.10391035, 2023.

https://doi.org/10.5194/gmd-2023-236
Preprint. Discussion started: 8 January 2024

Ye F, Zhang Y, Friedrichs M, Wang HV, Irby I, Shen J, Wang Z., A 3D, cross-scale, baroclinic model with implicit vertical transport for the Upper Chesapeake Bay and its tributaries. Ocean Model 107:82–96. https://doi.org/10.1016/j.ocemod.2016.10.004,2016.

Zampieri, L., Goessling, H. F., & Jung, T. Bright Prospects for Arctic Sea Ice Prediction on Subseasonal Time Scales. In Geophysical Research Letters (Vol. 45, Issue 18, pp. 9731–9738). https://doi.org/10.1029/2018gl079394, 2018

Zampieri, L., Kauker, F., Fröhle, J., Sumata, H., Hunke, E. C., and Goessling, H. F.: Impact of Sea-Ice Model Complexity on the Performance of an Unstructured-Mesh Sea-Ice/Ocean Model under Different Atmospheric Forcings, Journal of Advances in Modeling Earth Systems, 13, https://doi.org/10.1029/2020MS002438, 2021.

Zeng, X., Zhao, M., & Dickinson, R. E. Intercomparison of bulk aerodynamic algorithms for the computation of sea surface fluxes using TOGA COARE and TAO data. Journal of Climate, 11(10), 2628-2644. https://doi.org/10.1175/1520-0442(1998)011%3C2628:IOBAAF%3E2.0.CO;2, 1998.

Zhang, D., Jiang, C., Liang, D., and Cheng, L.: A review on TVD schemes and a refined flux-limiter for steady-state calculations, Journal of Computational Physics, 302, 114-154, https://doi.org/10.1016/j.jcp.2015.08.042, 2015.

Zhang, Y. J., Ateljevich, E., Yu, H. C., Wu, C. H., & Jason, C. S. A new vertical coordinate system for a 3D unstructured-grid model. Ocean Modelling, 85, 16-31. https://doi.org/10.1016/j.ocemod.2014.10.003, 2015.

Zhang, Y. J., Ye, F., Stanev, E. V., and Grashorn, S.: Seamless cross-scale modeling with SCHISM, Ocean Modelling, 102, 64-81, https://doi.org/10.1016/j.ocemod.2016.05.002, 2016.

Zhang, Y. J., Wu, C., Anderson, J., Danilov, S., Wang, Q., Liu, Y., and Wang, Q.: Lake ice simulation using a 3D unstructured grid model, Ocean Dynamics, 73, 219-230, https://doi.org/10.1007/s10236-023-01549-9, 2023.

Zhang, Z., Song, Z.-y., Guo, F., Zhang, D., Wen, Y.-n., and Hu, D.: Comparison and modification: TVD schemes for scalar transport on an unstructured grid, China Ocean Engineering, 30, 615-626, https://doi.org/10.1007/s13344-016-0039-1, 2016.

Zhang, Z., Song, Z.-y., Kong, J., and Hu, D.: A newr-ratio formulation for TVD schemes for vertex-centered FVM on an unstructured mesh, International Journal for Numerical Methods in Fluids, 81, 741-764, https://doi.org/10.1002/fld.4206, 2016.